

Article

Investigation on the Reaction Behaviour of Partially Reduced Iron under Blast Furnace Conditions

Gi-Ho La , Joon-Sung Choi  and Dong-Joon Min * 

Department of Materials Science and Engineering, Yonsei University, 50 Yonsei-Ro, Seodaemun-Gu, Seoul 03722, Korea; reduction@yonsei.ac.kr (G.-H.L.); melts@yonsei.ac.kr (J.-S.C.)

* Correspondence: chemical@yonsei.ac.kr; Tel.: +82-2-2123-2840

Abstract: The reaction behaviour of partially reduced iron (PRI) was studied to understand the effect of PRI utilisation in the blast furnace process. For quantitative analysis, the reaction behaviour of PRI under typical operating conditions of a blast furnace was measured using the thermogravimetric method along with the reduction behaviour of hematite and sinter. Experimental results indicated that the reoxidation behaviour of the PRI under the conditions of the upper shaft of the blast furnace retarded the indirect reduction rate in the lower shaft. The rate constants derived from the grain model, experimental results of scanning electron microscopy, and porosimetry analysis indicated that the phenomenon of reduction retardation of PRI under the conditions of the lower shaft originated owing to the reoxidation of PRI, resulting in the blockage of pores. The reaction behaviour considering the reaction characteristics of PRI was derived under conventional blast furnace conditions.

Keywords: blast furnace; partially reduced iron (PRI); kinetics; reoxidation



Citation: La, G.-H.; Choi, J.-S.; Min, D.-J. Investigation on the Reaction Behaviour of Partially Reduced Iron under Blast Furnace Conditions. *Metals* **2021**, *11*, 839. <https://doi.org/10.3390/met11050839>

Academic Editor: Pasquale Cavaliere

Received: 15 April 2021

Accepted: 14 May 2021

Published: 20 May 2021

Publisher's Note: MDPI stays neutral with regard to jurisdictional claims in published maps and institutional affiliations.



Copyright: © 2021 by the authors. Licensee MDPI, Basel, Switzerland. This article is an open access article distributed under the terms and conditions of the Creative Commons Attribution (CC BY) license (<https://creativecommons.org/licenses/by/4.0/>).

1. Introduction

The blast furnace process is a carbonaceous reduction process that has long been considered a representative ironmaking process with high energy efficiency. However, owing to the increasing demand for CO₂ mitigation due to the ongoing climate crisis, various theoretical studies have been conducted to achieve CO₂ mitigation, some of which include the improvement of process efficiency. The specific carbon rate according to various blast furnace operating conditions was evaluated using a Rist operating diagram, using which the critical carbon rate of 390 kg-C/t-HM was derived [1]. It has been reported that the specific carbon rate using a low-SiO₂ sinter [2] and Ca-rich coke [3] also has a limit of 371 kg-C/t-HM.

The reaction behaviour of iron-bearing materials under hydrogenous conditions has been investigated to overcome the current efficiency limit of the carbonaceous ironmaking process. The reduction rate of hematite by H₂ is approximately three times greater than the reduction rate by CO in the range of 1073–1223 K owing to the high effective diffusivity of H₂ gas molecules [4]. The reduction rate of wustite by a CO-H₂ gas mixture increases nonlinearly with an increase in the H₂ ratio [5]. It was reported that the reduction rate of wustite was enhanced by approximately 1.2 times owing to the water–gas shift reaction [6]. The reducing gas utilisation ratio, investigated using a blast furnace shaft inner reaction simulator, depended on the water gas shift reaction and gasification of carbon [7]. The possibility of utilising H₂ to lower CO₂ emissions and the changes in the specific carbon rate according to the H₂ injection rate were evaluated by heat and mass balance during the operation of the blast furnace [8]. It is generally accepted that the rate of the reduction reaction is enhanced with the H₂ injection rate. However, the imbalance of heat and mass should be considered.

Recently, several studies on CO₂ mitigation by pre-reduced iron-bearing materials, such as direct reduced iron (DRI), hot briquetted iron (HBI), and scrap, have also been reported [9]. The specific carbon rate, which is evaluated by the heat and mass balance of

the blast furnace, can be reduced by the pre-reduction of iron-bearing materials [10–12]. However, considering that the possibility of reoxidation of metallic iron exists owing to the relatively high oxygen potential conditions in the upper shaft, the reoxidation phenomenon of DRI and HBI was also reported to occur under the conditions of the upper shaft [13,14]. The rate-controlling step in the reoxidation of freshly reduced iron is the transition of an interfacial chemical reaction to solid-state diffusion with the increase of temperature owing to the formation of an oxide film [15]. In addition, the reoxidation rate of porous metallised iron pellets under high-temperature conditions is highly dependent on pore characteristics. The physical properties of the oxides formed during the reoxidation have a decisive impact on the subsequent reaction behaviour [16]. Many previous studies have pointed out that changes in physicochemical properties due to the reoxidation reaction should be considered when applying pre-reduced iron-bearing materials to blast furnace operations.

Partially reduced iron (PRI) could be produced using by-product gases of relatively low reduction potential for producing HBI. The utilization of PRI can efficiently mitigate the specific carbon rate of the iron-making process. Although macroscopic studies on the reoxidation behaviour of HBI and DRI under the conditions of a blast furnace have been reported, studies on the effect of the reaction behaviour of PRI on the specific carbon rate of a blast furnace have not been elucidated in detail. Therefore, the present study aims to quantitatively investigate the reaction behaviour of PRI under the conditions of a typical blast furnace and the effect of reoxidation of PRI.

2. Materials and Methods

2.1. Sample Preparation

The reaction behaviour of hematite (reagent grade, Fe₂O₃, >99.0%, Kanto) under the conditions of a typical blast furnace was set as the standard and compared with the reaction characteristics of sinter and PRI. The composition of the iron-bearing materials was evaluated using inductively coupled plasma-optical emission spectroscopy (735ICP-OES, Agilent, Santa Clara, CA, USA) and a K₂Cr₂O₇ titration method (JIS M8212: 2005) [17,18]. The initial degree of reduction of the iron-bearing materials was calculated using Equation (1):

$$R_t(\%) = 100 \times \left[1 - \frac{\left\{ \left(W_{Fe^{2+}}^0 \cdot \frac{MW_O}{MW_{Fe}} + W_{Fe^{3+}}^0 \cdot \frac{3 \cdot MW_O}{2 \cdot MW_{Fe}} \right) - W_t \right\}}{W_{T.Fe}^0 \cdot \frac{3 \cdot MW_O}{2 \cdot MW_{Fe}}} \right], \quad (1)$$

where R_t is the degree of reduction at time t (%), W_i^0 is the weight of species i in the initial state (g), W_t is the weight change of the iron-bearing materials at time t (g), and MW_i is the molar weight of species i (g/mol).

Table 1 lists the chemical composition and initial degree of reduction of the iron-bearing materials used in this study. To acquire homogeneous physical properties, the samples used in this study were crushed into a powder with a particle size of less than 100 µm using a ball mill (Pulverisette23, Fritsch, Idar-Oberstein, Germany). The powdered iron-bearing materials were then pressed in a cylindrical mould (height: 4 mm, diameter: 10 mm) under a force of 30,000 N with the addition of 10 wt% H₂O as a binder. All compacts produced were dried at 393 K in a dry oven for 24 h under an air atmosphere to remove H₂O.

Table 1. Chemical analysis of raw materials used in the present study.

Raw Material	Chemical Composition (wt%)						Initial Degree of Reducticon (%)
	T.Fe	Fe ²⁺	M.Fe	CaO/MgO	SiO ₂	Al ₂ O ₃	
Hematite	69.94	–	0.14	–	–	–	0.20
Sinter	58.01	3.91	0.24	10.26	5.47	1.99	2.66
PRI	75.07	46.83	23.78	0.12	6.11	3.41	52.47

2.2. Experiments

Figure 1 shows the conditions of a typical blast furnace based on a theoretical study on the reaction behaviour of iron oxide in a blast furnace [19] and the results measured by vertical sondes in a conventional blast furnace [1]. The temperature of the iron-bearing materials increases upon descent into the shaft zone, and the oxygen potential of the reducing gas reaches the Fe-FeO equilibrium condition in the thermal and chemical reserved zone (Stage I). Subsequently, the proportion of CO in the CO-CO₂ gas mixtures reached 1, which is known by the Boudouard reaction (Stage II).

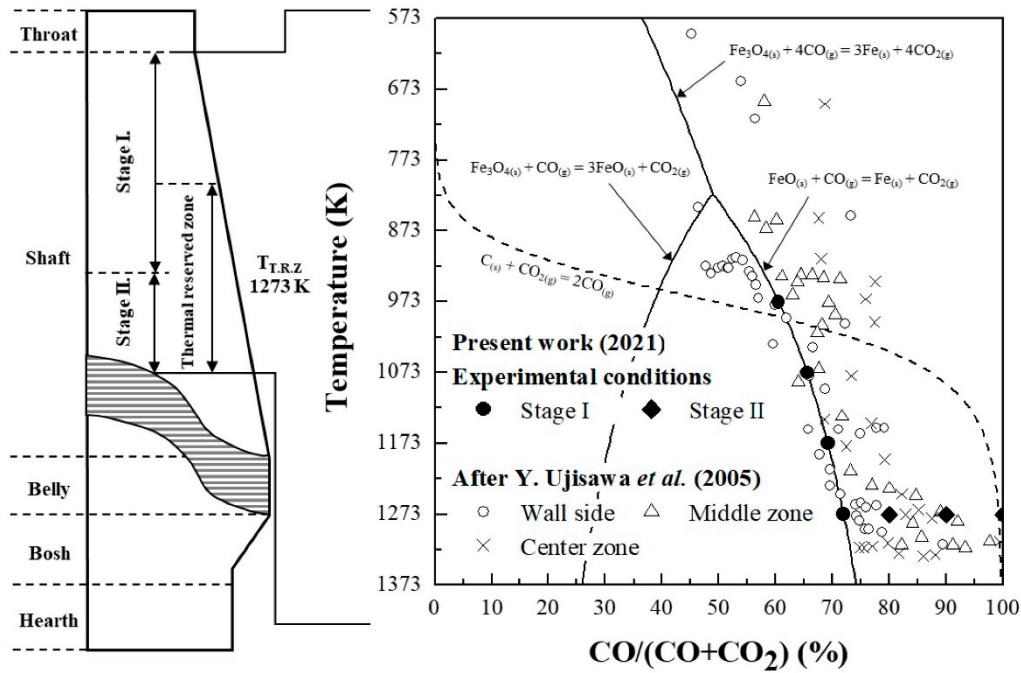


Figure 1. Schematic representation of experimental conditions of Stage I and Stage II with reduction conditions of a conventional blast furnace.

The iron-bearing material compact was reduced using a thermogravimetric analyser (TGA, SETSYS Evolution, Setaram, Caluire-et-Cuire, France), as shown in Figure 2, under the experimental conditions listed in Table 2. To evaluate the reaction behaviour of the iron-bearing compact under the conditions of Stage I, the compact was heated (50 K/min) under a N₂ atmosphere and converted to a reducing gas (N₂-CO-CO₂) after reaching the target temperature. The reaction behaviour of the iron-bearing compact under the conditions of Stage II was evaluated by converting the gas composition after the completion of Stage I at 1273 K. The composition of the gas was controlled using a mass flow controller (FC-280SA, Mykrolis, Billerica, MA, USA). After completion of the reaction, the compact was quenched (>50 K/min) to 298 K under a N₂ atmosphere. The physicochemical properties of the compacts were analysed using backscattered electron scanning microscopy (JSM-7800F, JEOL, Tokyo, Japan) and porosimetry (PM33GT, Quantachrome, Boynton Beach, FL, USA).

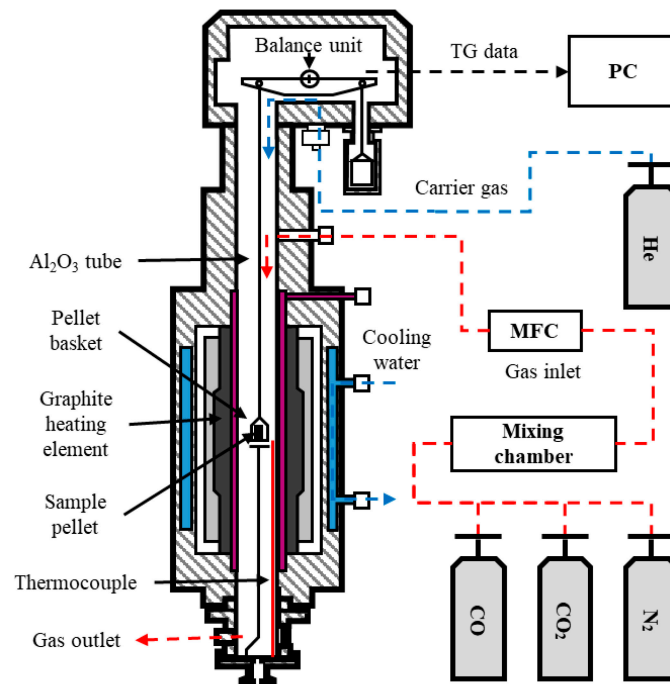


Figure 2. Schematic representation of the experimental apparatus.

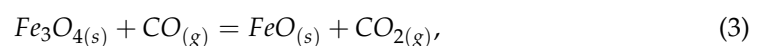
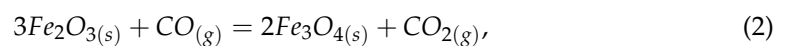
Table 2. Experimental conditions for the simulated blast furnace in the present study.

Stage	No.	Temperature (K)	Gas Composition (%)			
			N ₂	CO	CO ₂	CO/(CO + CO ₂)
Stage I (Fe/FeO equilibrium)	1	973	55.00	27.23	17.77	60.50
	2	1073	55.00	29.49	15.51	65.54
	3	1173	55.00	31.14	13.86	69.21
	4	1273	55.00	32.38	12.62	71.95
Stage II	5	1273	55.00	36.00	9.00	80.00
	6	1273	55.00	40.50	4.50	90.00
	7	1273	55.00	45.00	0.00	100.00

3. Results and Discussion

3.1. Reaction Behaviour of Iron Oxide in Shaft Zone of Blast Furnace

Figure 3 shows the reaction behaviour of hematite, sinter, and PRI under the experimental conditions of Stage I. Hematite and sinter of low reduction degree were reduced. PRI of high reduction degree processed oxidation. It was confirmed that the reaction behaviour of hematite and sinter is consistent with that reported in previous studies [1,19,20]. The reduction rate of the sinter was higher than that of hematite. Hematite and sinter were reduced to wustite according to Equations (2) and (3).



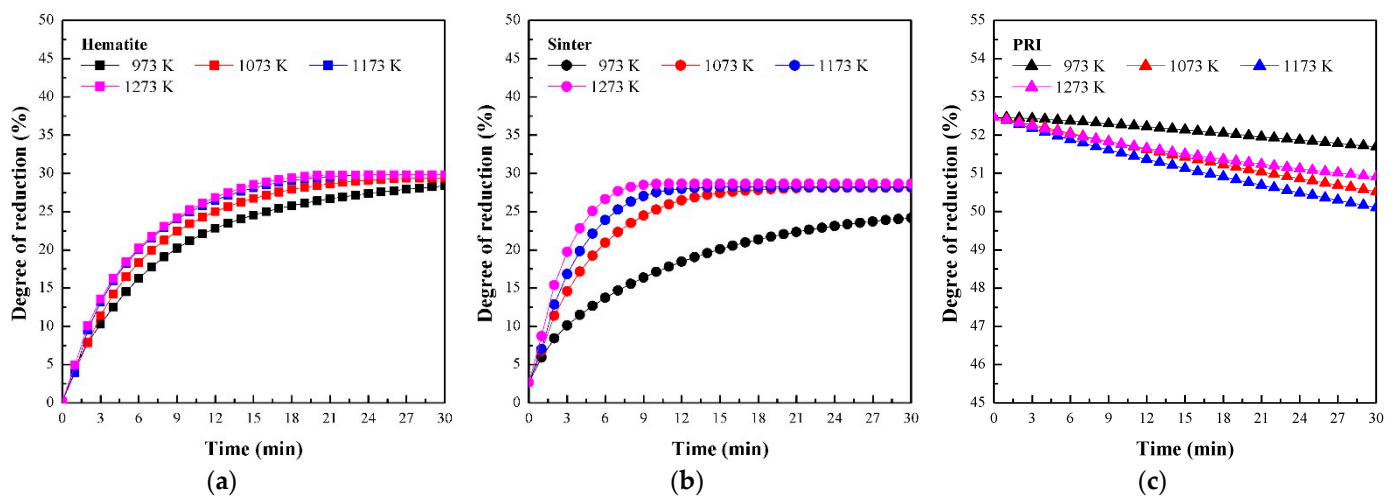


Figure 3. Reaction behaviour of (a) hematite, (b) sinter, and (c) PRI under the experimental conditions of Stage I.

However, the reoxidation of PRI was observed approximately 2 wt% of the degree of reduction according to Equation (4), which was similar to previous reports on the reaction behaviour of DRI and HBI under the conditions of the upper shaft [13,14].

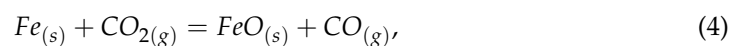


Figure 4 shows the reduction behaviour of hematite, sinter, and PRI under the experimental conditions of Stage II. The reaction rate in Stage II increased with increasing concentration of CO in the CO-CO₂ gas mixtures. The reduction rate of sinter shows a high reduction rate, followed by hematite and PRI. Notably, the PRI with a high initial reduction degree has the slowest reaction rate and lowest final degree of reduction, despite the high initial degree of reduction in Stage II.

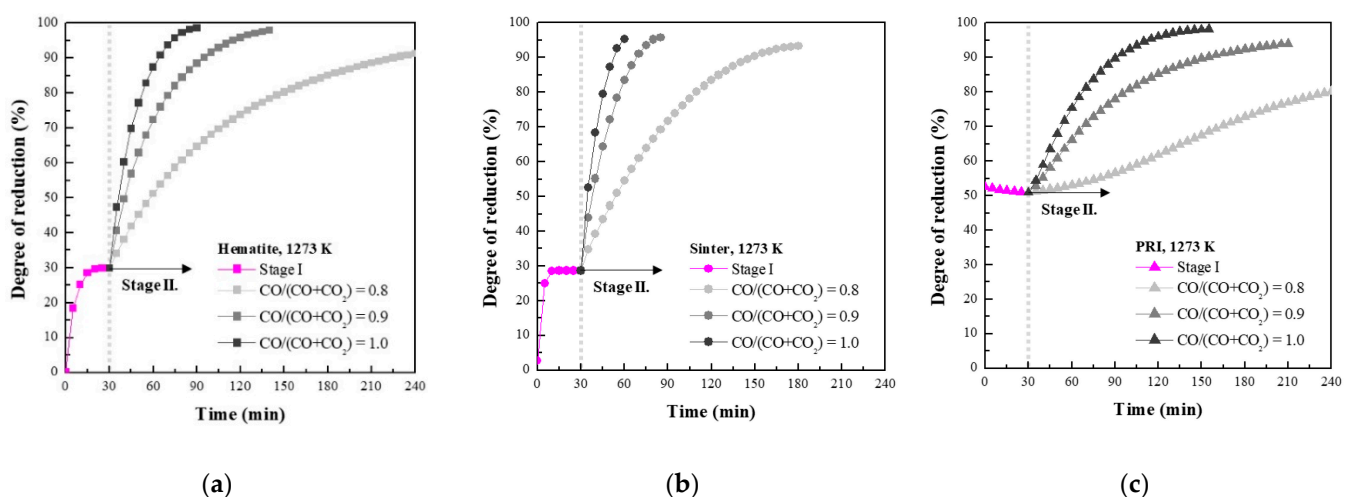


Figure 4. Reaction behaviour of (a) hematite, (b) sinter, and (c) PRI under the experimental conditions of Stage II.

The grain model [21] has been known as a general model for the analysis of gas–solid reaction kinetics. The iron-bearing material compact used in this study was reduced under the conditions of Stage I and Stage II respectively and assumed that shows a simple phase boundary during the reduction. The grain model was applied to quantitatively evaluate the reaction behaviour of iron-bearing materials and determine the rate-controlling step. The apparent rate constants of each mechanism were evaluated by a slope of the relationship

between the degree of reduction and the time. The relationship between the degree of reduction and the time for each rate-controlling step is represented below.

(a) Interfacial chemical reaction:

$$g(X_t) = 1 - (1 - X_t)^{1/3} = t^* = k_1 \cdot t = Y, \quad (5)$$

(b) Gaseous mass transport through the product layer (internal diffusion):

$$p(X_t) = \left(1 - (1 - X_t)^{1/3}\right)^2 = t^* / \hat{\sigma}_s^2 = k_2 \cdot t = Y, \quad (6)$$

(c) Mixed controlled (interfacial chemical reaction + internal diffusion) reaction:

$$t^* = g(X_t) + \hat{\sigma}_s^2 \cdot p(X_t) = k_3 \cdot t = Y, \quad (7)$$

where X_t is the fractional degree of reduction at time t ($R_t = 100 \cdot X_t$), t^* is the dimensionless time, $\hat{\sigma}_s^2$ is the shrinking core modulus ($\hat{\sigma}_s^2 = k_1/k_2$), and k_1 , k_2 , and k_3 are the apparent rate constants (1/s). The shrinking core modulus represents the ratio of the capacities of chemical reaction and diffusion based on the grain model. The relative resistance between the interfacial reaction and internal diffusion was evaluated according to Equations (8) and (9) to determine the rate-controlling step.

$$\eta_i = \frac{1}{1 + \hat{\sigma}_s^2}, \quad (8)$$

$$\eta_d = \frac{\hat{\sigma}_s^2}{1 + \hat{\sigma}_s^2}, \quad (9)$$

The results listed in Table 3 show that the rate-controlling steps of the reduction reaction of Stage I were controlled by internal diffusion, and that of Stage II were controlled by the interfacial chemical reaction and internal diffusion, respectively.

Table 3. Relative resistance between interfacial reaction and internal diffusion under experimental conditions in the present study.

Sample	Stage	Temperature (K)	CO/(CO + CO ₂) (%)	Shrinking Core Modulus ($\hat{\sigma}_s^2$)	Interfacial Reaction Resistance (η_i)	Internal Diffusion Resistance (η_d)	Rate Determining Step
Hematite	I. (Fe/FeO equilibrium)	973	60.50	7.0511	0.1242	0.8758	Internal Diffusion (D3)
		1073	65.54	7.2263	0.1216	0.8784	
		1173	69.21	7.1028	0.1234	0.8766	
		1273	71.95	7.1840	0.1222	0.8778	
	II.	1273	80.00	1.2925	0.4362	0.5638	Mixed (R3 + D3)
		1273	90.00	1.0941	0.4775	0.5225	
Sinter	I. (Fe/FeO equilibrium)	973	60.50	7.8171	0.1134	0.8866	Internal Diffusion (D3)
		1073	65.54	7.2175	0.1217	0.8783	
		1173	69.21	7.4243	0.1187	0.8813	
		1273	71.95	7.4144	0.1188	0.8812	
	II.	1273	80.00	1.3227	0.4305	0.5695	Mixed (R3 + D3)
		1273	90.00	1.2083	0.4528	0.5472	
PRI	I. (Fe/FeO equilibrium)	973	60.50	2.2978	0.3032	0.6968	Internal Diffusion (D3)
		1073	65.54	2.3341	0.2999	0.7001	
		1173	69.21	2.3483	0.2987	0.7013	
		1273	71.95	2.3255	0.3007	0.6993	
	II.	1273	80.00	1.4151	0.4141	0.5859	Mixed (R3 + D3)
		1273	90.00	1.1232	0.4170	0.5290	
		1273	100.00	0.9290	0.5184	0.4816	

Figure 5a shows the changes in k_2 under the conditions of Stage I. The positive k_2 values of hematite and sinter indicate that reduction occurred. In contrast, the k_2 value of the PRI was negative, indicating oxidation. Figure 5b shows the changes in k_3 for Stage II. The reaction rate of wustite produced from hematite in this experiment is quantitatively consistent with the results of a previous study on the effect of CO concentration in CO-CO₂ gas mixtures on the reduction rate of wustite produced from hematite and calcium ferrite [22].

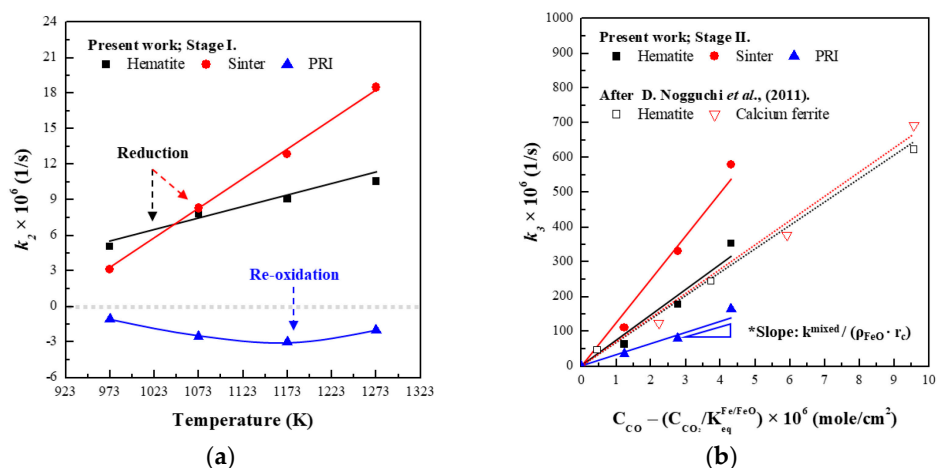


Figure 5. Changes in (a) k_2 in Stage I and (b) k_3 in Stage II (k_2 : controlled by gaseous mass transport through the product layer; k_3 : mixed controlled).

The effective diffusivity of gas (Stage I) and the mixed controlled rate constant (Stage II) evaluated using the grain model are presented in Table 4. The activation energy of the reduction of hematite to wustite calculated from the temperature dependence of the effective diffusivity in Figure 6a is approximately 27.85 kJ/mol, which is consistent with the activation energy of 28.88 kJ/mole of the initial reduction of hematite [23]. In contrast, the effective diffusivity of PRI increased with increasing temperature and exhibited an inflexion point at approximately 1173 K. A decrease in the oxidation rate at high temperatures has also been reported in previous studies on the reoxidation of iron. Furthermore, it has been reported that a decrease in the reoxidation occurs at high temperatures owing to the decrease in porosity caused by sintering of metallic iron [15] and the decrease in the diffusion rate due to the change in pore characteristics upon reoxidation [16].

Table 4. Effective diffusivity and mixed controlled rate constants of hematite, sinter, and PRI under experimental conditions in the present study.

Sample	Stage	Temperature (K)	Effective Diffusivity, D_e (cm/s)	Mixed Controlled Rate Constant, k_m (1/s)
Hematite	I. (Fe/FeO equilibrium)	973	8.643×10^{-4}	–
		1073	1.350×10^{-3}	–
		1173	1.629×10^{-3}	–
		1273	1.977×10^{-3}	–
	II.	1273	–	1.180
Sinter	I. (Fe/FeO equilibrium)	973	4.350×10^{-4}	–
		1073	1.172×10^{-3}	–
		1173	1.883×10^{-3}	–
		1273	2.828×10^{-3}	–
	II.	1273	–	1.854
PRI	I. (Fe/FeO equilibrium)	973	3.314×10^{-4}	–
		1073	9.168×10^{-4}	–
		1173	1.254×10^{-3}	–
		1273	9.508×10^{-4}	–
	II.	1273	–	0.470

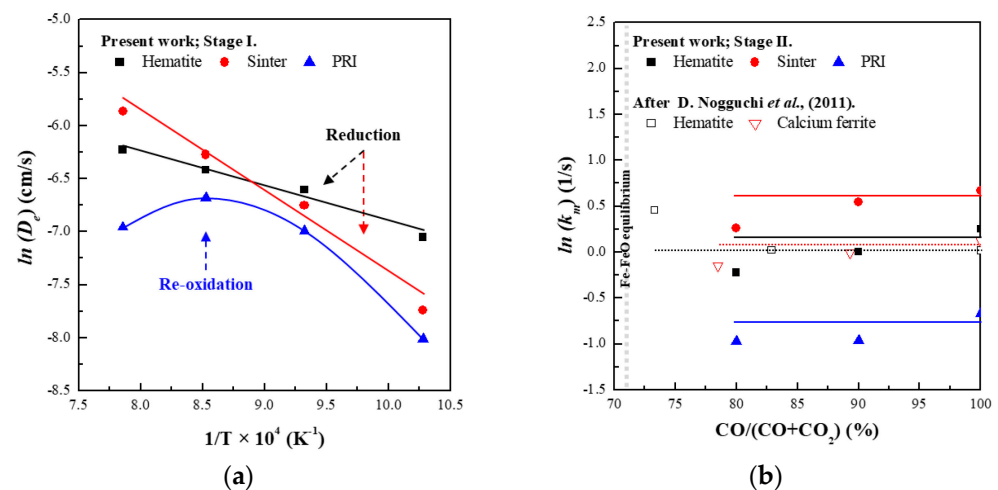


Figure 6. Changes in (a) effective diffusivity in Stage I and (b) mixed controlled rate constant in Stage II.

The mixed controlled rate constant of Stage II in Figure 6b indicates the retardation phenomenon of the PRI in Stage II. The relationship between the rate constant of hematite and that of sinter was qualitatively consistent with the results of previous studies, which indicated that the rate of reduction was dominated by porosity [24,25]. Therefore, it can be reasonably assumed that the retardation of PRI in Stage II is due to changes in physicochemical properties determined by the reoxidation of PRI under the conditions of Stage I [26].

3.2. Analysis of Morphology and Porosity of PRI

To evaluate the effect of the physicochemical properties of the oxides on the reaction behaviour, the morphology after the reaction was evaluated. Figure 7 shows backscattered electron SEM (BSE-SEM, JSM-7800F, JEOL, Tokyo, Japan) images of the iron-bearing material after reaction under the conditions of Stage I. The apparent porosity of hematite and sinter tends to increase as the temperature increases [24,25]. However, the apparent porosity of PRI initially increased with increasing temperature from 937 to 1173 K and showed a dense morphology at 1273 K.

The changes in porosity, effective diffusivity, and molar volume owing to the reoxidation under the conditions of Stage I are shown in Figure 8. The porosity of PRI was evaluated using mercury porosimeter. The molar volume change during the oxidation of iron ($\Delta V_{Fe-FeO}^{oxidation}$) was estimated using Equation (10) [27]:

$$\Delta V_{Fe-FeO}^{oxidation} = V_{FeO} - V_{Fe} \quad (10)$$

where $\Delta V_{Fe-FeO}^{oxidation}$ is the molar volume change during oxidation of iron ($cm^3/mole$) and V_i is the molar volume of species i ($cm^3/mole$).

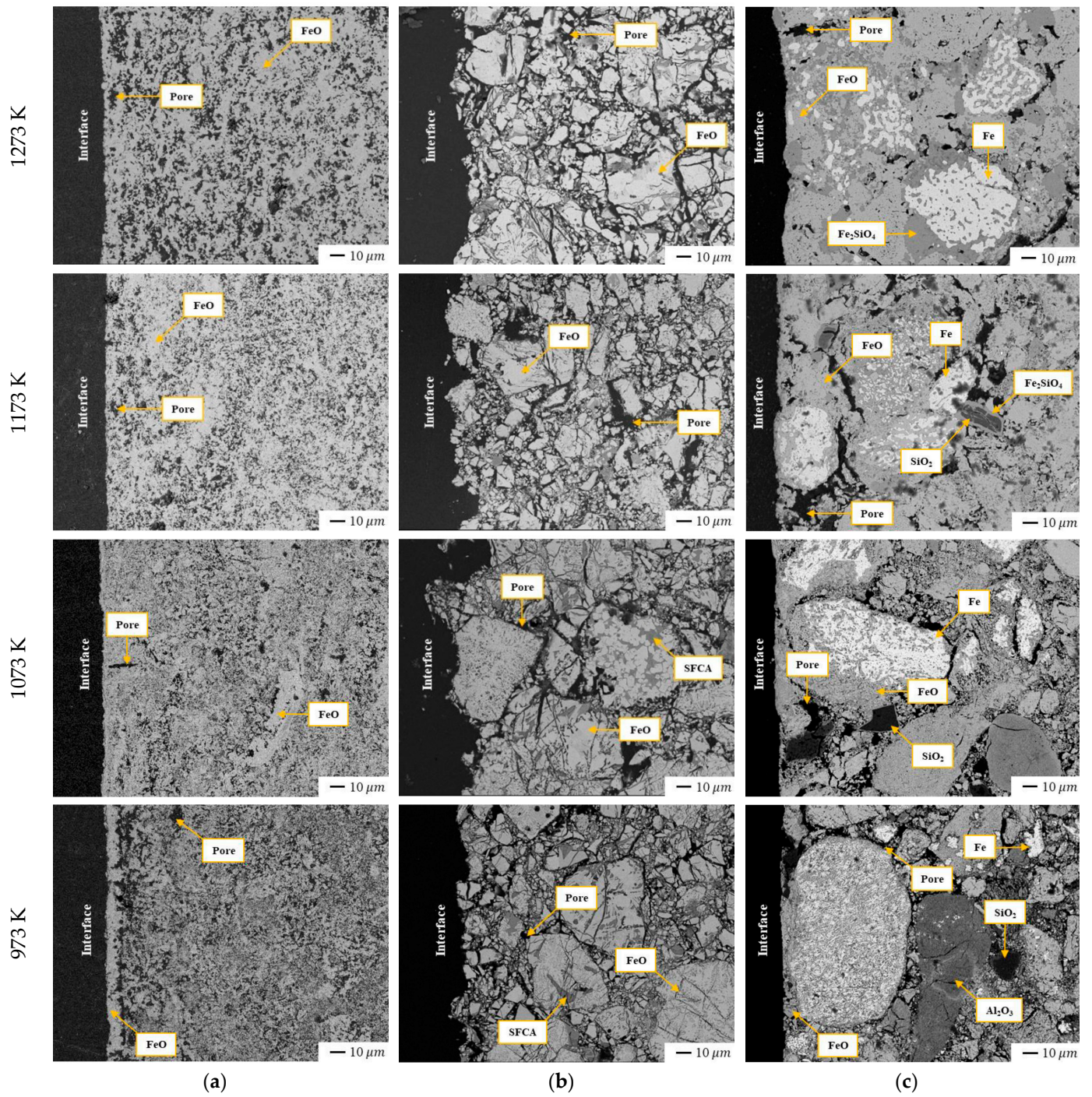


Figure 7. BSE-SEM images of (a) hematite, (b) sinter, and (c) PRI after the reaction under the experimental conditions of Stage I.

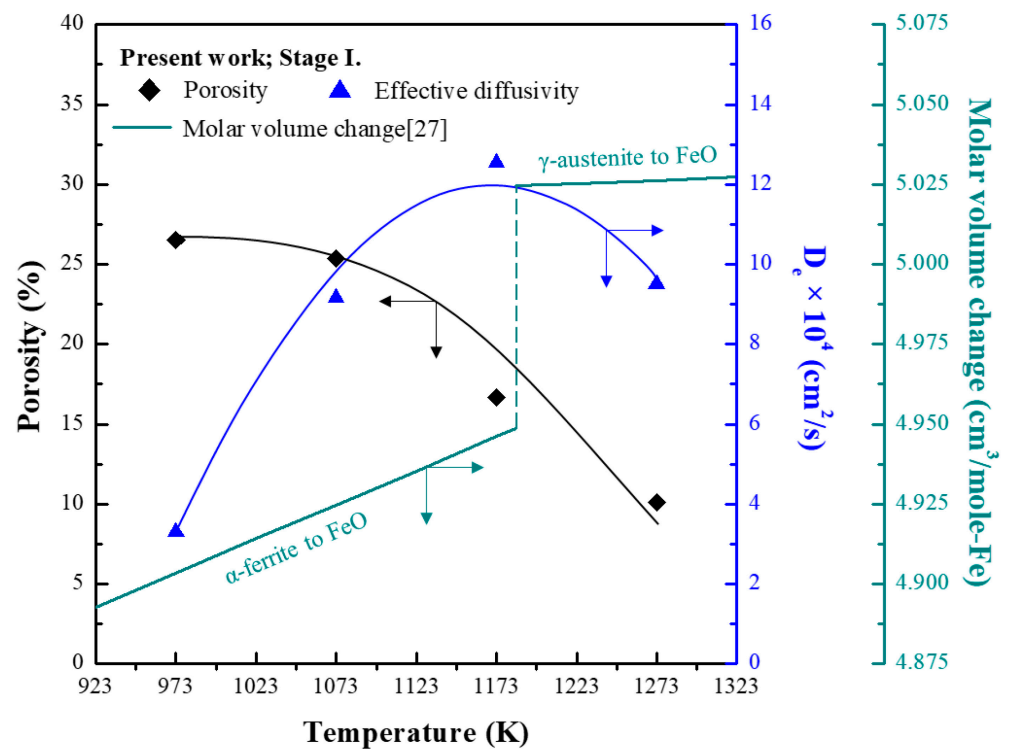


Figure 8. Porosity, effective diffusivity, and molar volume change during oxidation of PRI after the reaction under the experimental conditions of Stage I.

The porosity of PRI decreases as the temperature increases, and it can be seen that the porosity of PRI decreases rapidly under temperature conditions near 1173 K. The molar volume change due to oxidation increases significantly at 1189 K (A3), where a phase transition between alpha-iron and gamma-iron occurs [27]. Therefore, the decrease in the reoxidation rate of PRI at 1273 K under the conditions of Stage I is due to the blockage of pores resulting from a significant increase in the molar volume changes during oxidation according to the phase transition of metallic iron.

3.3. Reaction Behaviour of PRI

Figure 9 shows the reaction behaviour of oxides under the conditions of a typical blast furnace [1,19,28]. The apparent rate constants of Stage I ($k_2^{approx.}$) and Stage II ($k_3^{approx.}$) were derived from the effective diffusivity and the mixed controlled rate constants listed in Table 4. Additionally, the changes in the degree of reduction of the iron-bearing materials for Stage I and Stage II were calculated using Equations (6) and (7), respectively.

In Stage I, the reduction of hematite and sinter occurred, while the reoxidation of PRI proceeded. The reduction rate of sinter in Stage II was faster than that of hematite, which is consistent with previous studies [24,25]. However, PRI shows a slow reduction rate with a low final degree of reduction due to the retardation phenomenon caused by the blockage of pores during the reoxidation reaction in Stage I, despite the high initial degree of reduction.

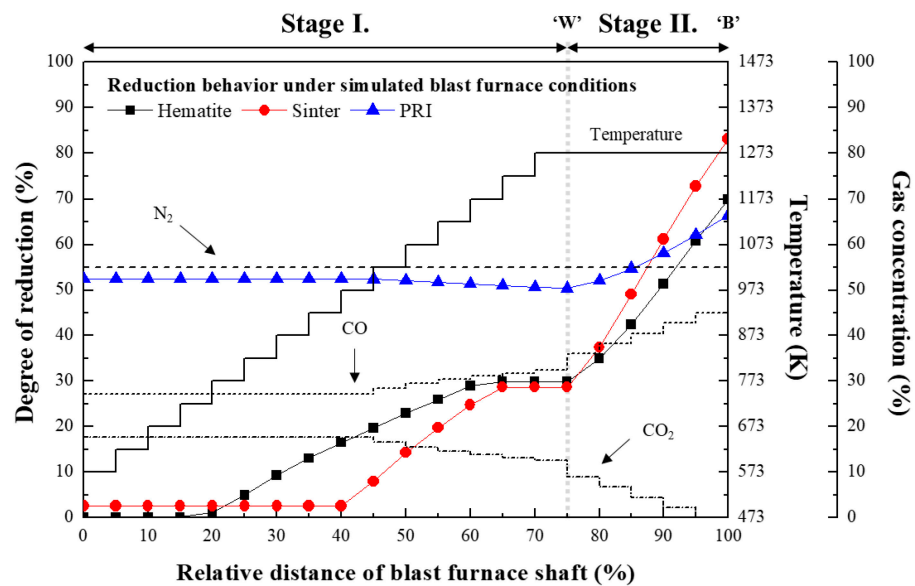
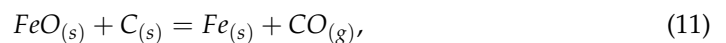


Figure 9. Reaction behaviour of hematite, sinter, and PRI under the simulated blast furnace conditions.

It has been reported that the specific carbon rate decreases with the charging of pre-reduced iron-bearing materials without the reoxidation phenomenon [10–12]. Considering the reduction retardation phenomenon due to the reoxidation of PRI, an imbalance in the degree of reduction of each iron-bearing material in the cohesive zone can occur and deteriorate the stability of the blast furnace operation. In particular, the reduction in the cohesive zone after Stage II proceeds by direct reduction, which is an endothermic reaction, as shown in Equation (11) [19].



Consequently, an additional amount of carbon for direct reduction is required compared with the specific carbon rate without considering the reoxidation of PRI. It can be reasonably speculated that the reduction retardation phenomenon of PRI owing to reoxidation in Stage I negatively impacts the gas utilisation and heat balance of the blast furnace. Therefore, the reaction behaviour, including the reoxidation and reduction retardation of pre-reduced iron-bearing materials, and the prevention of reoxidation, including the optimisation of the pre-reduction degree of PRI, carbon composite, and the utilization of hydrogen, should be considered for the effective utilisation of PRI in the blast furnace.

4. Conclusions

The effect of the reaction behaviour of PRI on the specific carbon rate and CO₂ emissions was evaluated using the Rist operating diagram. The results of this study can be summarised as follows:

- (1) PRI was reoxidised, whereas hematite and sinter were reduced in Stage I. The rate of reoxidation initially increased with increasing temperature and then decreased at 1273 K owing to the blockage of pores resulting from the significant increase in the molar volume changes during oxidation according to the phase transition of metallic iron.
- (2) The reduction rate of PRI in Stage II is retarded. It was confirmed that the reduction retardation of PRI was caused by a blockage of pores owing to the reoxidation of PRI that occurred in Stage I.
- (3) The reaction behaviour of the oxides was evaluated based on the effective diffusivity and mixed controlled rate constant. It was confirmed that the reaction behaviour of hematite in this study is consistent with the reaction behaviour of the ferrous burden in the theoretical blast furnace.

- (4) The degree of reduction of PRI at the final stage of Stage II is lower than that of hematite owing to the reduction retardation phenomenon of PRI. Consequently, the reduction retardation phenomenon of the PRI could deteriorate the stability of the blast furnace operation and negatively impact the heat balance and gas utilisation of the blast furnace.

Author Contributions: Investigation, data curation, writing—original draft preparation, G.-H.L.; methodology, J.-S.C.; conceptualization, supervision, D.-J.M.; All authors have read and agreed to the published version of the manuscript.

Funding: Not applicable.

Data Availability Statement: Data sharing not applicable.

Acknowledgments: This work was supported by the Korea Institute of Energy Technology Evaluation and Planning (KETEP) and the Ministry of Trade, Industry & Energy (MOTIE) of the Republic of Korea (No. 20172010106300), the Korea Initiative for fostering the University of Research and Innovation (KIURI) Program of National Research Foundation (NRF) funded by the Korean government (MSIT) (No. NRF-2020M3H1A1077207), and the Brain Korea 21 FOUR Project in 2021 (BK21).

Conflicts of Interest: The authors declare no conflict of interest.

References

- Ujisawa, Y.; Nakano, K.; Matsukura, Y.; Sunahara, K.; Komatsu, S.; Yamamoto, T. Subjects for achievement of blast furnace operation with low reducing agent rate. *ISIJ Int.* **2005**, *45*, 1379–1385. [[CrossRef](#)]
- Matsukura, Y.; Nakano, K.; Sunahara, K.; Ujisawa, Y.; Yamamoto, K. Effect of burden properties on permeability in blast furnace. *Iron Steel* **2001**, *87*, 350–356. [[CrossRef](#)]
- Nomura, S.; Ayukawa, H.; Kitaguchi, H.; Tahara, T.; Matsuzaki, S.; Naito, M.; Koizumi, S.; Ogata, Y.; Nakayama, T.; Abe, T. Improvement in blast furnace reaction efficiency through the use of highly reactive calcium rich coke. *ISIJ Int.* **2005**, *45*, 316–324. [[CrossRef](#)]
- Moon, I.J.; Rhee, C.H.; Min, D.J. Reduction of hematite compacts by H₂-CO gas mixtures. *Steel Res.* **1998**, *69*, 302–306. [[CrossRef](#)]
- El-Geassy, A.A.; Rajakumar, V. Gaseous reduction of wustite with H₂, CO and H₂-CO mixtures. *Trans. Iron Steel Inst. Jpn.* **1985**, *25*, 449–458. [[CrossRef](#)]
- Usui, T.; Kawabata, H.; Ono-Nakazato, H.; Kurosaka, A. Fundamental experiments on the H₂ gas injection into the lower part of a blast furnace shaft. *ISIJ Int.* **2002**, *42* (Suppl. S14), S14–S18. [[CrossRef](#)]
- Park, T.J.; Lee, J.H.; Kim, D.G.; Kim, H. Estimation of the H₂ Gas Utilization Ratio Using a BF Shaft Inner Reaction Simulator. *Metall. Mater. Trans. B* **2020**, *51*, 417–421. [[CrossRef](#)]
- Kim, W.H.; Min, D.J. A mass and energy estimation for the hydrogen utilization in the iron-making process. *Sci. China Technol. Sci.* **2011**, *54*, 1655–1660. [[CrossRef](#)]
- Sundar Murti, N.S.; Seshadri, V. Kinetics of reduction of synthetic chromite with carbon. *Trans. Iron Steel Inst. Jpn.* **1982**, *22*, 925–933. [[CrossRef](#)]
- Rist, A.; Meysson, N. A dual graphic representation of the blast-furnace mass and heat balances. *J. Mater.* **1967**, *19*, 50–59. [[CrossRef](#)]
- Ono, Y. Rist operating diagram (I). *Iron Steel* **1993**, *79*, N618. [[CrossRef](#)]
- Ono, Y. Rist operating diagram (II). *Iron Steel* **1993**, *79*, N711–N715. [[CrossRef](#)]
- Kaushik, P.; Fruehan, R. Behavior of direct reduced iron and hot briquetted iron in the upper blast furnace shaft: Part I. Fundamentals of kinetics and mechanism of oxidation. *Metall. Mater. Trans. B* **2006**, *37*, 715–725. [[CrossRef](#)]
- Kaushik, P.; Fruehan, R. Behavior of direct reduced iron and hot briquetted iron in the upper blast furnace shaft: Part II. A model of oxidation. *Metall. Mater. Trans. B* **2006**, *37*, 727–732. [[CrossRef](#)]
- El-Geassy, A.A.; El-Kashif, F.O.; Nasr, M.I.; Omar, A.A. Kinetics and mechanisms of re-oxidation of freshly reduced iron compacts. *ISIJ Int.* **1994**, *34*, 541–547. [[CrossRef](#)]
- Taniguchi, S.; Ohmi, M.; Nakaoka, S. Re-oxidation behaviour of a porous metallised iron pellet at relatively high temperatures. *Trans. Jpn. Inst. Met.* **1981**, *22*, 145–152. [[CrossRef](#)]
- Yang, L.; Belton, G. Iron redox equilibria in CaO-Al₂O₃-SiO₂ and MgO-CaO-Al₂O₃-SiO₂ slags. *Metall. Mater. Trans. B* **1998**, *29*, 837–845. [[CrossRef](#)]
- Park, Y.; Min, D.J. Effect of iron redox equilibrium on the foaming behavior of MgO-saturated slags. *Metall. Mater. Trans. B* **2018**, *49*, 1709–1718. [[CrossRef](#)]
- Biswas, A.K. *Principles of Blast Furnace Ironmaking: Theory and Practice*; Cootha Publishing House: Brisbane, Australia, 1981.
- Turkdogan, E. Blast furnace reactions. *Metall. Trans. B* **1978**, *9*, 163–179. [[CrossRef](#)]
- Szekely, J. *Gas-Solid Reactions*, 1st ed.; Academic Press: New York, NY, USA, 1976.

22. Noguchi, D.; Ohno, K.I.; Maeda, T.; Nishioka, K.; Shimizu, M. Effect of CO gas concentration on reduction rate of major mineral phase in sintered iron ore. *J. Iron Steel Inst. Jpn.* **2011**, *97*, 548–553. [[CrossRef](#)]
23. Nasr, M.I.; Omar, A.A.; Hessian, M.M.; El-Geassy, A.A. Carbon monoxide reduction and accompanying swelling of iron oxide compacts. *ISIJ Int.* **1996**, *36*, 164–171. [[CrossRef](#)]
24. Mousa, E.A. Effect of basicity on wüstite sinter reducibility under simulated blast furnace conditions. *Ironmak. Steelmak.* **2014**, *41*, 418–429. [[CrossRef](#)]
25. Kim, W.-H.; Lee, Y.-S.; Suh, I.-K.; Min, D.-J. Influence of CaO and SiO₂ on the reducibility of wüstite using H₂ and CO gas. *ISIJ Int.* **2012**, *52*, 1463–1471. [[CrossRef](#)]
26. Corbari, R.; Fruehan, R. Reduction of iron oxide fines to wustite with CO/CO₂ gas of low reducing potential. *Metall. Mater. Trans. B* **2010**, *41*, 318–329. [[CrossRef](#)]
27. McCammon, C.; Liu, L.-G. The effects of pressure and temperature on nonstoichiometric wüstite, Fe_xO: The iron-rich phase boundary. *Phys. Chem. Miner.* **1984**, *10*, 106–113. [[CrossRef](#)]
28. Mizoguchi, H.; Suzuki, H.; Hayashi, S. Influence of mixing coal composite iron ore hot briquettes on blast furnace simulated reaction behavior in a packed mixed bed. *ISIJ Int.* **2011**, *51*, 1247–1254. [[CrossRef](#)]